Phase coexistence in polydisperse charged hard-sphere fluids: Mean spherical approximation

Yurij V. Kalyuzhnyi
Institute for Condensed Matter Physics, Svientsitskoho 1, 79011 Lviv, Ukraine
and Center for Computational Materials Science and Institut für Theoretische Physik, TU Wien,
Wiedner Hauptstraße 8-10, A-1040 Wien, Austria

Gerhard Kahl
Center for Computational Materials Science and Institut für Theoretische Physik, TU Wien,
Wiedner Hauptstraße 8-10, A-1040 Wien, Austria

Peter T. Cummings
Department of Chemical Engineering, Vanderbilt University, Nashville, Tennessee 37235-1604
and Chemical Sciences Division, Oak Ridge National Laboratory, Oak Ridge, Tennessee 27831-6110

Taking advantage of the availability of the analytic solution of the mean spherical approximation for a mixture of charged hard spheres with an arbitrary number of components we show that the *polydisperse* fluid mixture of charged hard spheres belongs to the class of truncatable free energy models, i.e., to those systems where the thermodynamic properties can be represented by a finite number of (generalized) moments of the distribution function that characterizes the mixture. Thus, the formally infinitely many equations that determine the parameters of the two coexisting phases can be mapped onto a system of coupled nonlinear equations in these moments. We present the formalism and demonstrate the power of this approach for two systems; we calculate the full phase diagram in terms of cloud and shadow curves as well as binodals and discuss the distribution functions of the coexisting daughter phases and their charge distributions. © *2004 American Institute of Physics.* [DOI: 10.1063/1.1737291]

I. INTRODUCTION

The existence of the liquid-gas phase transition in a binary mixture of charged hard spheres (CHS) with same diameter σ and opposite charges ($z_+ = -z_-$), i.e., the so-called symmetric restricted primitive model (RPM) of electrolytes, has been predicted more than three decades ago both theoretically[1–3] as well as in computer simulation methods.[4] However, results stemming from the different methods for the location of the critical point were rather controversial and only during the last decade—due to the substantial advance achieved in computer simulation methodology and in computational power—an accurate location of the coexistence curve and of the critical point has been gradually achieved.[5–12] The corresponding theoretical predictions are still by far less satisfactory: only in recent years several theoretical methods[13–19] have been developed, which are able to predict a qualitative or sometimes even a quantitative description of the RPM phase diagram. Probably one of the most accurate one among these[19] is based on the associative mean spherical approximation[20,21] (AMSA) (or the so-called binding MSA): it combines the AMSA and the simple interpolation scheme (SIS) introduced by Stell and Zhou.[22] While this approach gives a reasonably accurate estimate for the location of the critical point, its prediction for the overall shape of the phase diagram (as it is also the case for the other theoretical approaches mentioned above) is rather poor.

Despite these problems for the symmetric RPM, more recent theoretical and computer simulation studies were dedicated to a binary CHS mixture with charge- and/or size-asymmetry.[11,23–31] While for such systems both theoretical and computer simulation studies were performed, the next step towards a ternary mixture was limited—as a consequence of the high complexity of the problem—to theoretical studies, most of them realized within the mean spherical approximation (MSA) (see the review of Caccamo,[32] and references therein).

In this work we proceed to the polydisperse case, i.e., to a mixture of CHS with formally an infinite number of components. Similar as in a previous study on a hard sphere Yukawa (HSY) mixture[33] our investigations are based on the mean spherical approximation (MSA), taking benefit of the availability of the analytic solution of this liquid state theory for a mixture of CHS with an arbitrary number of components.[34,35] As done in most approaches used at present to study polydisperse systems we characterize each of the infinitely many components of the system by a (continuous) variable ξ, which is distributed according to a distribution function $F(\xi)$; it should be noted that ξ can also be a set of variables. This parameter thus takes over the role of the set of discrete concentrations $\{c_i\}$ in a mixture with a *finite* number of components. This function $F(\xi)$ is positive and normalized, i.e., $\int d\xi F(\xi) = 1$. $F(\xi_0)d\xi$ represents thus the fraction of particles in a polydisperse mixture with the parameter ξ located in an interval of width $d\xi$ around ξ_0.

In this contribution we want to investigate the phase be-

10133

havior of a polydisperse fluid mixture of CHS. Let $F^{(0)}(\xi)$ and $\rho^{(0)}$ be the distribution function and the density of the parent phase, then we are looking for the distribution functions of the coexisting daughter phases, $F^{(\alpha)}(\xi)$, $\alpha=1, 2$ (here we restrict ourselves to two-phase equilibria): these functions, along with the coexistence densities $\rho^{(1)}$ and $\rho^{(2)}$ are sufficient to determine all properties of the daughter phases. The main problem when dealing with the phase behavior in polydisperse mixtures is the fact that we are now faced with a formally infinite number of coexistence equations for the two daughter phases: e.g., the Helmholtz free energy is now defined in a space of infinite dimensionality, which makes the task of building the common tangent plane construction intractable. On the level of the coexistence equations of equal pressure and chemical potentials of the coexisting phases at fixed temperature T this means that one has to solve the infinitely many equations

$$P^{(1)}=P^{(2)} \quad \mu^{(1)}(\xi)=\mu^{(2)}(\xi) \quad \text{for all } \xi. \quad (1)$$

Solution of this problem for a general system, where P and the $\mu(\xi)$ have to be calculated numerically (with some suitable liquid state theory) remain up to date yet unsolved.[36] However, for a few models it is possible to circumvent this problem successfully: this applies for those systems where the thermodynamic properties can be expressed—within a certain liquid state approximation—by a finite number of generalized moments of the distribution function $F(\xi)$;[37] models that belong to this class are called "truncatable free energy models." In those cases it is then possible to map the phase equilibrium conditions for a polydisperse mixture (1) onto a system of coupled nonlinear equations for the corresponding generalized moments of the distribution functions $F^{(\alpha)}(\xi)$ of the coexisting phases.

Historically, the simplest, nontrivial truncatable free energy model is the generalization of the van der Waals model to the case of a polydisperse mixture; the model was already proposed by Gualtieri et al.[38] and was exploited later in detail by Bellier-Castella et al.[39,40] In particular these authors studied the *full* phase behavior of polydisperse fluid mixtures, i.e., they determined the cloud and shadow curves as well as the binodals. Further investigations for this system can be found in Ref. 36. Searching for other truncatable free energy models that go beyond the mean field level, two of the authors encountered the polydisperse HSY mixture within the MSA which has been studied in detail in Ref. 33. Again the coexistence Eqs. (1) could be mapped onto a coupled system of nonlinear equations for the unknown (generalized) moments of the daughter distribution functions. The higher level of sophistication of this model with respect to the van der Waals model has brought along a considerable increase in the complexity of the formalism and of the numerical treatment: under the assumption of factorizable Yukawa interactions, twenty-two equations for the unknown moments had to be solved.

In the present paper we extend this formalism to study the phase behavior of the polydisperse CHS fluid. Although the development of the formalism draws on parallels from the HSY case,[33] the situation is more complex, since we now have to take into account additional constraints, such as the

charge neutrality, and the distribution functions of each phase contain contributions due to the positive and negative charge. We finally arrive at fifteen coupled nonlinear equations for the unknown generalized moments of the daughter distribution functions $F^{(\alpha)}(\xi)$, $\alpha=1, 2$. Dealing with a hard core system the obvious choice for the variable ξ is the HS diameter σ and we have two quantities that can be distributed independently according to respective distribution functions: the size σ and the charge z of the particles; thus, $F(\xi)=F(\sigma,z)$. Although expressions can be presented for the two independently distributed system parameters, the formalism turns out to be considerably complex. Thus we have used the simplifying assumption, that the charge of the particles is proportional to their surface, i.e., an ansatz which seems physically sound. We point out that this reduction to only one independent system parameter was only done with respect to a more compact presentation of the formalism and to a justifiable numerical effort.

To demonstrate the power and applicability of the concept we present results for two polydisperse fluids mixtures: the first one is a straightforward polydisperse generalization of the RPM, the other one is a polydisperse extension of a 1:1 electrolyte primitive model with an asymmetry in the HS sizes. We present results for the full phase diagrams (cloud and shadow curves as well as binodals) discussing characteristic features of the daughter distribution functions and the charge distributions between the coexisting phases. For reasons outlined in the paper we have restricted ourselves to beta-distributions for the parent distribution functions.

The paper is organized as follows: in the subsequent section we present the theory (starting from the case of a mixture with a finite number of components and generalizing to the polydisperse case). In Sec. III we present the results of the two systems investigated and close the paper with concluding remarks.

II. THE THEORY

A. Phase equilibrium conditions

We start with the simple case of an n-component mixture of charged particles which we consider at a temperature $T[\beta=(k_BT)^{-1}]$ placed in a continuum with a dielectric constant ϵ. Each species i has the charge ez_i and the number density $\rho_i^{(0)}=N_i^{(0)}/V^{(0)}$, where $N_i^{(0)}$ is the number of the particles of type i, e is the elementary charge, and $V^{(0)}$ is the volume of the system. Henceforward, the upper index (0) will denote properties of the parent phase whose phase behavior we intend to study. The system is neutral, so that the following relation is satisfied:

$$\sum_{i=1}^{n} z_i N_i^{(0)}=0. \quad (2)$$

We assume that at a certain temperature T the system separates into m daughter phases where each phase α is characterized by a volume $V^{(\alpha)}$ and a number of particles of species i, $N_i^{(\alpha)}$. Hereafter we will denote a set of quantities $y_1^{(\alpha)}$, $y_2^{(\alpha)},...,y_n^{(\alpha)}$ by $\{y_i^{(\alpha)}\}$.

At equilibrium these parameters take values which minimize the total Helmholtz free energy of the system $\Sigma_{\alpha=1}^m A^{(\alpha)}(T,V^{(\alpha)},\{N_i^{(\alpha)}\})$ and satisfy the following set of constraints:

(i) charge neutrality

$$\sum_{i=1}^n z_i N_i^{(\alpha)}=0; \tag{3}$$

(ii) total volume conservation

$$V^{(0)}=\sum_{\alpha=1}^m V^{(\alpha)}; \tag{4}$$

(iii) conservation of the total number of the particles of each i species

$$N_i^{(0)}=\sum_{\alpha=1}^m N_i^{(\alpha)}. \tag{5}$$

Application of the Lagrange multiplier method gives the following phase equilibrium conditions for the pressure P and for the chemical potentials μ_i of component i in the coexisting phases α and β,

$$P^{(\alpha)}(T,V^{(\alpha)},\{N_i^{(\alpha)}\})=P^{(\beta)}(T,V^{(\beta)},\{N_i^{(\beta)}\}), \tag{6}$$

$$\mu_i^{(\alpha)}(T,V^{(\alpha)},\{N_i^{(\alpha)}\})+(1-\delta_{\alpha\alpha_0})\lambda^{(\alpha)}z_i$$
$$=\mu_i^{(\beta)}(T,V^{(\beta)},\{N_i^{(\beta)}\})+(1-\delta_{\beta\alpha_0})\lambda^{(\beta)}z_i$$
$$\alpha,\beta=1,...,m \quad \text{and} \quad i=1,...,n. \tag{7}$$

Here $\lambda^{(\alpha)}$ is the Lagrange multiplier introduced to satisfy the charge neutrality condition (3). Due to the overall neutrality of the system, Eq. (2), this constraint is imposed on each phase α, except one arbitrarily chosen phase α_0. Solution of the set of Eqs. (3) (for $\alpha\neq\alpha_0$), (4)–(7) yields phase coexisting values for $\lambda^{(\alpha)}$ ($\alpha\neq\alpha_0$), $V^{(\alpha)}$, and $\{N_i^{(\alpha)}\}$.

For the sake of further extension of the phase equilibrium conditions (3)–(7) to the polydisperse case it is more convenient to use the set of variables represented by the density of phase α, $\rho^{(\alpha)}=N^{(\alpha)}/V^{(\alpha)}$, and by the fractions $x_i^{(\alpha)}=N_i^{(\alpha)}/N_i^{(0)}$ and $x^{(\alpha)}=N^{(\alpha)}/N^{(0)}$ with $N^{(\alpha)}=\Sigma_{i=1}^n N_i^{(\alpha)}$. In terms of these variables we have

$$P^{(\alpha)}(T,\rho^{(\alpha)},\{x_i^{(\alpha)}\})=P^{(\beta)}(T,\rho^{(\beta)},\{x_i^{(\beta)}\}), \tag{8}$$

$$\mu_i^{(\alpha)}(T,\rho^{(\alpha)},\{x_i^{(\alpha)}\})+(1-\delta_{\alpha\alpha_0})\lambda^{(\alpha)}z_i$$
$$=\mu_i^{(\beta)}(T,\rho^{(\beta)},\{x_i^{(\beta)}\})+(1-\delta_{\beta\alpha_0})\lambda^{(\beta)}z_i, \tag{9}$$

$$x_i^{(0)}=\sum_{\alpha=1}^m x_i^{(\alpha)}x^{(\alpha)}, \tag{10}$$

$$v^{(0)}=\sum_{\alpha=1}^m v^{(\alpha)}x^{(\alpha)}, \tag{11}$$

$$\sum_{i=1}^n z_i x_i^{(\alpha)}=0, \quad \alpha(\neq\alpha_0)=1,...,m, \tag{12}$$

$$\sum_{i=1}^n x_i^{(\alpha)}=1, \quad \alpha=1,...,m, \tag{13}$$

where $v^{(0)}=1/\rho^{(0)}$ and $v^{(\alpha)}=1/\rho^{(\alpha)}$. Relations (10), (11), and (12) express the conservation of the total number of particles of each species i, conservation of the total system volume, and the charge neutrality condition for each phase $\alpha(\neq\alpha_0)$, respectively.

Now, extension of the phase equilibrium conditions (8)–(13) to the polydisperse case is rather straightforward and can be achieved by switching from the discrete index variable i to a continuous index variable ξ by using the following substitution rule[42]

$$x_i\rightarrow F(\xi)d\xi, \tag{14}$$

$F(\xi)$ being a positive distribution function normalized to 1. It should be pointed out that ξ now stands for the variables $\{\sigma,z\}$. Due to this substitution, summations over i in Eqs. (8)–(13) become integrations over ξ; further, thermodynamic properties become *functionals* of the distribution function $F(\xi)$ which we will indicate by square brackets:

$$P^{(\alpha)}(T,\rho^{(\alpha)};[F^{(\alpha)}])=P^{(\beta)}(T,\rho^{(\beta)};[F^{(\beta)}]), \tag{15}$$

$$\mu^{(\alpha)}(\xi,T,\rho^{(\alpha)};[F^{(\alpha)}])+(1-\delta_{\alpha\alpha_0})\lambda^{(\alpha)}z(\xi)$$
$$=\mu^{(\beta)}(\xi,T,\rho^{(\beta)};[F^{(\beta)}])+(1-\delta_{\beta\alpha_0})\lambda^{(\beta)}z(\xi), \tag{16}$$

$$F^{(0)}(\xi)=\sum_{\alpha=1}^m F^{(\alpha)}(\xi)x^{(\alpha)}, \tag{17}$$

$$v^{(0)}=\sum_{\alpha=1}^m v^{(\alpha)}x^{(\alpha)}, \tag{18}$$

$$\int z(\xi)F^{(\alpha)}(\xi)d\xi=0, \quad \alpha(\neq\alpha_0)=1,...,m, \tag{19}$$

$$\int F^{(\alpha)}(\xi)d\xi=1, \quad \alpha=1,...,m. \tag{20}$$

Formally the set of relations (15)–(20) form a closed set of equations for the unknowns $\rho^{(\alpha)}$, $x^{(\alpha)}$, $\lambda^{(\alpha)}$, and $F^{(\alpha)}(\xi)$ which can be solved as soon as expressions for the thermodynamical properties of the corresponding polydisperse system at hand will be available.

At present this problem seems to be solvable only for the so-called truncatable free energy models, i.e., these models, for which thermodynamic properties can be represented by a finite number of (generalized) moments of the distribution function $F(\xi)$. Formally, polydisperse mixtures of CHS where the thermodynamical properties are calculated within the MSA belong to the family of truncatable free energy models. In the subsequent section we will present the extension of the MSA expressions for the Helmholtz free energy, for the pressure, and for the chemical potentials from a mixture of a finite number of components of CHS to the polydisperse case.

B. Thermodynamic properties

We consider again the n-component mixture of CHS discussed in the previous section. The pair potential of the model is of the form

10136   J. Chem. Phys., Vol. 120, No. 21, 1 June 2004

Kalyuzhnyi, Kahl, and Cummings

$$\Phi_{ij}(r) = \begin{cases} \infty & r \leqslant \sigma_{ij} \\ e^2 z_i z_j / \epsilon r & \sigma_{ij} < r < \infty \end{cases}, \tag{21}$$

where the σ_i are the HS diameters of the particles of type i and $\sigma_{ij} = (\sigma_i + \sigma_j)/2$.

The MSA solution for a mixture of CHS and the corresponding expressions for the Helmholtz free energy, A, and the pressure, P, for the model at hand had been obtained earlier:[34,35]

$$\beta \frac{(A - A^{(HS)})}{V} = \frac{\Gamma^3}{3\pi} + \beta \frac{E^{(ex)}}{V}, \tag{22}$$

$$\beta(P - P^{(HS)}) = -\frac{\Gamma^3}{3\pi} - \frac{1}{2} \pi \beta^* \left(\frac{D}{\Delta}\right)^2; \tag{23}$$

$E^{(ex)}$ is the excess internal energy and in the following summations over i range from 1 to n:

$$\beta \frac{E^{(ex)}}{V} = -\beta^* \left(\frac{\pi \Omega D^2}{2\Delta} + \Gamma \sum_i \frac{\rho_i z_i^2}{1 + \sigma_i \Gamma} \right), \tag{24}$$

$$\Omega = 1 + \frac{\pi}{2\Delta} \sum_i \frac{\rho_i \sigma_i^3}{1 + \sigma_i \Gamma}, \tag{25}$$

$$D = \frac{1}{\Omega} \sum_i \frac{\rho_i z_i \sigma_i}{1 + \sigma_i \Gamma}. \tag{26}$$

$\beta^* = e^2 \beta / \epsilon$, $\Delta = 1 - (\pi/6)\zeta_3$, $\zeta_3 = \Sigma_i \rho_i \sigma_i^3$, and Γ is the solution of the nonlinear algebraic equation

$$\Gamma^2 = \pi \beta^* \sum_i \rho_i \left(\frac{z_i - \pi \sigma_i^2 D/2\Delta}{1 + \sigma_i \Gamma} \right)^2. \tag{27}$$

Expressions for the chemical potentials μ_i can be obtained using the standard relation $\mu_i = (\partial A / \partial \rho_i)_{\beta, \rho_{j \neq i}}$ and taking into account the stationary property of the MSA Helmholtz free energy, $\partial A / \partial \Gamma = 0$. A simple calculation leads to the following expression:

$$\beta(\mu_i - \mu_i^{(HS)}) = -\frac{\beta^*}{1 + \sigma_i \Gamma} \left\{ \Gamma z_i^2 + \frac{\pi}{2\Delta} \sigma_i D \right.$$
$$\left. \times \left[2z_i + \frac{\pi}{6\Delta} \sigma_i^2 D(\sigma_i \Gamma - 2) \right] \right\}. \tag{28}$$

All thermodynamical properties of the *polydisperse* mixture of the charged HS model can be simply obtained from the expressions (22)–(28) by using prescription (14). Since for the model at hand each species is defined by its size (σ) and its charge (z), we can replace the variable ξ in Eq. (14) by the pair of continuous random variables σ and z, distributed according to the probability distribution function $F(\sigma, z) \geqslant 0$ with

$$\int_0^\infty d\sigma \int_{-\infty}^\infty dz F(\sigma, z) = 1. \tag{29}$$

Upon this substitution the expressions for the Helmholtz free energy (22) and for the pressure (23) will be unchanged. For the excess internal energy $E^{(ex)}$ and for the chemical potentials $\mu(\sigma, z)$, which are now functions of σ and z, we have

$$\beta \frac{E^{(ex)}}{V} = -\beta^* \left[\frac{\pi \Omega D^2}{2\Delta} \right.$$
$$\left. + \Gamma \rho \int_0^\infty d\sigma \int_{-\infty}^\infty dz \frac{z^2}{1 + \sigma \Gamma} F(\sigma, z) \right], \tag{30}$$

$$\beta[\mu(\sigma, z) - \mu^{(HS)}(\sigma)] = -\frac{\beta^*}{1 + \sigma \Gamma} \left\{ \Gamma z^2 + \frac{\pi}{2\Delta} \sigma D \right.$$
$$\left. \times \left[2z + \frac{\pi}{6\Delta} \sigma^2 D(\sigma \Gamma - 2) \right] \right\}, \tag{31}$$

where Ω, D, and the generalized moments ζ_n are defined as follows:

$$\zeta_n = \rho \int_0^\infty d\sigma \int_{-\infty}^\infty dz \sigma^n F(\sigma, z), \tag{32}$$

$$\Omega = 1 + \frac{\pi}{2\Delta} \rho \int_0^\infty d\sigma \int_{-\infty}^\infty dz \frac{\sigma^3}{1 + \sigma \Gamma} F(\sigma, z), \tag{33}$$

$$D = \frac{1}{\Omega} \rho \int_0^\infty d\sigma \int_{-\infty}^\infty dz \frac{z\sigma}{1 + \sigma \Gamma} F(\sigma, z), \tag{34}$$

and Γ is obtained from the solution of the equation

$$\Gamma^2 = \pi \beta^* \rho \int_0^\infty d\sigma \int_{-\infty}^\infty dz \left(\frac{z - \pi \sigma^2 D/2\Delta}{1 + \sigma \Gamma} \right)^2 F(\sigma, z). \tag{35}$$

Thermodynamic properties of the corresponding polydisperse HS system can be calculated using the semiempirical expressions due to Mansoori et al.,[41] generalized to the polydisperse case.[33,42]

C. Two-phase coexistence

In this study we will restrict ourselves to the case where the polydisperse mixture of CHS [parent phase, denoted by "(0)"] separates in two phases only [daughter phases, denoted by "(1)" and "(2)"]; under these conditions the set of multiphase equilibrium conditions, Eqs. (15)–(20), becomes[33,39]

$$P^{(1)}(T, \rho^{(1)}; [F^{(1)}]) = P^{(2)}(T, \rho^{(2)}; [F^{(2)}]), \tag{36}$$

$$F^{(1)}(\sigma, z) = F^{(2)}(\sigma, z) \frac{\rho^{(2)}}{\rho^{(1)}} \exp\{\beta \Delta \tilde{\mu} + \lambda z\}, \tag{37}$$

$$\rho^{(2)} F^{(2)}(\sigma, z) = \frac{\rho^{(1)} - \rho^{(2)}}{\rho^{(1)} - \rho^{(0)}} \rho^{(0)} F^{(0)}(\sigma, z)$$
$$+ \frac{\rho^{(0)} - \rho^{(2)}}{\rho^{(0)} - \rho^{(1)}} \rho^{(1)} F^{(1)}(\sigma, z), \tag{38}$$

$$\int_0^\infty d\sigma \int_{-\infty}^\infty dz \, z F^{(2)}(\sigma, z) = 0, \tag{39}$$

$$\int_0^\infty d\sigma \int_{-\infty}^\infty dz \, F^{(\alpha)}(\sigma, z) = 1, \quad \alpha = 1 \text{ or } \alpha = 2, \tag{40}$$

where

J. Chem. Phys., Vol. 120, No. 21, 1 June 2004

Phase coexistence in a polydisperse fluid   10137

$$\Delta\tilde{\mu} = \tilde{\mu}^{(2)}(\sigma,z,T,\rho^{(2)};[F^{(2)}])$$
$$- \tilde{\mu}^{(1)}(\sigma,z,T,\rho^{(1)};[F^{(1)}]); \tag{41}$$

the $\tilde{\mu}^{(\alpha)}$, $\alpha=1$, 2 are the excess (over the ideal gas) chemical potentials and $\alpha_0=1$ (i.e., $\lambda=\lambda^{(2)}$). $\rho^{(0)}$ and $F^{(0)}(\sigma,z)$ denote the density and the distribution function of the parent phase, respectively. The relation between $F^{(0)}(\sigma,z)$ and two daughter phase distribution functions, $F^{(1)}(\sigma,z)$ and $F^{(2)}(\sigma,z)$, i.e., Eq. (38), follows from the condition of the conservation of the total number of particles of each species characterized by σ and z, Eq. (17), and the conservation of the total volume, Eq. (18).

A distribution $F^{(\alpha)}(\sigma,z)$ as introduced above allows an independent variation of the charge and of the size of the particles. However, to reduce the amount of numerical calculations we assume a distribution, which strongly correlates these two model parameters, i.e.,

$$F^{(\alpha)}(\sigma,z) = F_+^{(\alpha)}(\sigma,z) + F_-^{(\alpha)}(\sigma,z)$$

$$= F_+^{(\alpha)}(\sigma)\delta\left(z - z_+^{(0)}\frac{\sigma^2}{\langle\sigma^2\rangle_+^{(0)}}\right)$$

$$+ F_-^{(\alpha)}(\sigma)\delta\left(z - z_-^{(0)}\frac{\sigma^2}{\langle\sigma^2\rangle_-^{(0)}}\right) \quad \alpha=1,2, \tag{42}$$

where we have introduced the first and the second moments

$$\langle\sigma\rangle_\pm^{(\alpha)} = \int_0^\infty d\sigma\,\sigma f_\pm^{(\alpha)}(\sigma)$$

and

$$\langle\sigma^2\rangle_\pm^{(\alpha)} = \int_0^\infty d\sigma\,\sigma^2 f_\pm^{(\alpha)}(\sigma). \tag{43}$$

Our assumption is physically sound, since it states that the charge is proportional to the surface of the particles; from a more practical point of view assumption (42) reduces double integrals over σ and z in previous expressions to integrals over σ only.

Further we put

$$F_\pm^{(\alpha)}(\sigma) = \alpha_\pm^{(\alpha)} f_\pm^{(\alpha)}(\sigma), \tag{44}$$

where $\alpha_+^{(\alpha)}$ denotes the fraction of positive and $\alpha_-^{(\alpha)}$ the fraction of negative particles in the phase α

$$\alpha_\pm^{(\alpha)} = \int_0^\infty d\sigma F_\pm^{(\alpha)}(\sigma); \tag{45}$$

obviously, $\alpha_+^{(\alpha)} + \alpha_-^{(\alpha)} = 1$; in the following, the index $\pm$ will be a short-hand notation for quantities that characterize positive ($+$) or negative ($-$) particles. The partial probability distribution functions, $f_\pm^{(\alpha)}(\sigma)$, introduced in Eq. (44) are normalized

$$\int_0^\infty d\sigma f_\pm^{(\alpha)}(\sigma) = 1. \tag{46}$$

For the average charge of positive ($+$) or negative ($-$) particles in the phase α, $z_\pm^{(\alpha)}$, we obtain

$$z_\pm^{(\alpha)} = \int_0^\infty d\sigma \int_{-\infty}^\infty dz\, z F_\pm^{(\alpha)}(\sigma,z) = z_\pm^{(0)}\frac{\langle\sigma^2\rangle_\pm^{(\alpha)}}{\langle\sigma^2\rangle_\pm^{(0)}}. \tag{47}$$

The charge neutrality condition takes the following simple form:

$$z_+^{(\alpha)}\alpha_+^{(\alpha)} + z_-^{(\alpha)}\alpha_-^{(\alpha)} = 0, \quad \alpha=0,1,2. \tag{48}$$

Now the set of equations that determine phase equilibrium, Eqs. (36)–(40), can be recast in terms of the distribution functions $F_\pm^{(\alpha)}(\sigma)$

$$P^{(1)}(T,\rho^{(1)};[F_+^{(1)},F_-^{(1)}]) = P^{(2)}(T,\rho^{(2)};[F_+^{(2)},F_-^{(2)}]), \tag{49}$$

$$F_\pm^{(1)}(\sigma) = F_\pm^{(2)}(\sigma)\frac{\rho^{(2)}}{\rho^{(1)}}\exp\{\beta\Delta\tilde{\mu}_\pm + \lambda z_\pm(\sigma)\}, \tag{50}$$

$$\rho^{(2)}F_\pm^{(2)}(\sigma) = \frac{\rho^{(1)}-\rho^{(2)}}{\rho^{(1)}-\rho^{(0)}}\rho^{(0)}F_\pm^{(0)}(\sigma)$$

$$+ \frac{\rho^{(0)}-\rho^{(2)}}{\rho^{(0)}-\rho^{(1)}}\rho^{(1)}F_\pm^{(1)}(\sigma), \tag{51}$$

$$z_+^{(2)}\alpha_+^{(2)} + z_-^{(2)}\alpha_-^{(2)} = 0, \tag{52}$$

$$\int_0^\infty d\sigma\{F_+^{(\alpha)}(\sigma) + F_-^{(\alpha)}(\sigma)\} = 1, \quad \alpha=1 \quad \text{or} \quad \alpha=2, \tag{53}$$

where

$$\Delta\tilde{\mu}_\pm = \tilde{\mu}_\pm^{(2)}(\sigma,T,\rho^{(2)};[F_+^{(2)},F_-^{(2)}])$$
$$- \tilde{\mu}_\pm^{(1)}(\sigma,T,\rho^{(1)};[F_+^{(1)},F_-^{(1)}]) \tag{54}$$

and

$$z_\pm(\sigma) = z_\pm^{(0)}\sigma^2/\langle\sigma^2\rangle_\pm^{(0)}. \tag{55}$$

Equation (51) can be used to eliminate $F_\pm^{(2)}(\sigma)$ [or $F_\pm^{(1)}(\sigma)$] from Eq. (50) to give

$$F_\pm^{(\alpha)}(\sigma)$$

$$= F_\pm^{(0)}(\sigma)Q_\pm^{(\alpha)}(\sigma,T;\rho^{(0)},\rho^{(1)},\rho^{(2)};[F_+^{(\alpha)},F_-^{(\alpha)}]),$$

$$\alpha=1,2, \tag{56}$$

where

$$\rho^{(\alpha)}Q_{\pm}^{(\alpha)}(\sigma,T;\rho^{(0)},\rho^{(1)},\rho^{(2)};[F_+^{(1)},F_-^{(1)}]) = \frac{\rho^{(0)}(\rho^{(2)}-\rho^{(1)})\{1-\delta_{1\alpha}+\delta_{1\alpha}\exp[\beta\Delta\tilde{\mu}_{\pm}+\lambda z_{\pm}(\sigma)]\}}{(\rho^{(0)}-\rho^{(1)})-(\rho^{(0)}-\rho^{(2)})\exp[\beta\Delta\tilde{\mu}_{\pm}+\lambda z_{\pm}(\sigma)]},$$
$$\alpha=1,2. \tag{57}$$

Relations (49), (52), (53), and (56), along with Eq. (57), with $\alpha=1$ or $\alpha=2$, represent a closed set of equations to be solved for the unknowns $\rho^{(1)}$, $\rho^{(2)}$, λ, and $F_+^{(\alpha)}(\sigma)$, $\alpha=1$, 2. Since thermodynamic properties of the model at hand are defined by the finite number of generalized moments we can follow previous studies[33,39] and map this set of equations onto a closed set of fifteen algebraic equations for λ, $\rho^{(\alpha)}$, and $\Gamma^{(\alpha)}$, and for ten generalized moments $\zeta_n^{(\alpha)}$, $n=1,2,3$, $\Omega^{(\alpha)}$, $D^{(\alpha)}$, where α denotes the value of the corresponding quantity in phase α ($\alpha=1,2$). We have

$$\zeta_n^{(\alpha)} = \rho^{(\alpha)}\int_0^{\infty}d\sigma\sigma^n[F_+^{(0)}(\sigma)Q_+^{(\alpha)}(\sigma,T,\rho^{(0)};\mathcal{X})$$
$$+F_-^{(0)}(\sigma)Q_-^{(\alpha)}(\sigma,T,\rho^{(0)};\mathcal{X})],$$
$$n=1,2,3, \tag{58}$$

$$\Omega^{(\alpha)} = 1 + \frac{\pi\rho^{(\alpha)}}{2\Delta^{(\alpha)}}\int_0^{\infty}d\sigma\frac{\sigma^3}{1+\sigma\Gamma^{(\alpha)}}$$
$$\times[F_+^{(0)}(\sigma)Q_+^{(\alpha)}(\sigma,T,\rho^{(0)};\mathcal{X})$$
$$+F_-^{(0)}(\sigma)Q_-^{(\alpha)}(\sigma,T,\rho^{(0)};\mathcal{X})], \tag{59}$$

$$D^{(\alpha)} = \frac{\rho^{(\alpha)}}{\Omega^{(\alpha)}}\int_0^{\infty}d\sigma\frac{\sigma}{1+\sigma\Gamma^{(\alpha)}}$$
$$\times[z_+(\sigma)F_+^{(0)}(\sigma)Q_+^{(\alpha)}(\sigma,T,\rho^{(0)};\mathcal{X})$$
$$+z_-(\sigma)F_-^{(0)}(\sigma)Q_-^{(\alpha)}(\sigma,T,\rho^{(0)};\mathcal{X})], \tag{60}$$

where the unknowns of the problem are collected in set $\mathcal{X}$, i.e.,

$$\mathcal{X}=\{\rho^{(1)},\rho^{(2)},\lambda;[\Gamma^{(1)}\{\zeta_n^{(1)}\}\Omega^{(1)}D^{(1)}],$$
$$[\Gamma^{(2)}\{\zeta_n^{(2)}\}\Omega^{(2)}D^{(2)}]\}. \tag{61}$$

The remaining five equations are found from the equality of the pressure in both phases (36),

$$P^{(1)}(T,\rho^{(1)};[\Gamma^{(1)}\{\zeta_n^{(1)}\}\Omega^{(1)}D^{(1)}])$$
$$=P^{(2)}(T,\rho^{(2)};[\Gamma^{(2)}\{\zeta_n^{(2)}\}\Omega^{(2)}D^{(2)}]), \tag{62}$$

from the charge neutrality condition (52),

$$\int_0^{\infty}d\sigma\sigma^2 F_+^{(0)}(\sigma)\cdot\int_0^{\infty}d\sigma\sigma^2 F_+^{(0)}(\sigma)Q_+^{(2)}(\sigma,T,\rho^{(0)};\mathcal{X})$$
$$=\int_0^{\infty}d\sigma\sigma^2 F_-^{(0)}(\sigma)\cdot\int_0^{\infty}d\sigma\sigma^2 F_-^{(0)}(\sigma)Q_-^{(2)}(\sigma,T,\rho^{(0)};\mathcal{X}), \tag{63}$$

from the normalization condition (53) for either phase $\alpha=1$ or phase $\alpha=2$,

$$1 = \int_0^{\infty}d\sigma[F_+^{(0)}(\sigma)Q_+^{(\alpha)}(\sigma,T,\rho^{(0)};\mathcal{X})$$
$$+F_-^{(0)}(\sigma)Q_-^{(\alpha)}(\sigma,T,\rho^{(0)};\mathcal{X})] \tag{64}$$

and from Eq. (35), written for the scaling parameters $\Gamma^{(\alpha)}$ for each of the two phases,

$$\frac{(\Gamma^{(\alpha)})^2}{\pi\beta^*} = \rho^{(\alpha)}\int_0^{\infty}d\sigma\left[\left(\frac{z_+(\sigma)-\pi\sigma^2 D^{(\alpha)}/2\Delta^{(\alpha)}}{1+\sigma\Gamma^{(\alpha)}}\right)^2\right.$$
$$\times F_+^{(0)}(\sigma)Q_+^{(\alpha)}(\sigma,T,\rho^{(0)};\mathcal{X})$$
$$+\left(\frac{z_-(\sigma)-\pi\sigma^2 D^{(\alpha)}/2\Delta^{(\alpha)}}{1+\sigma\Gamma^{(\alpha)}}\right)^2$$
$$\left.\times F_-^{(0)}(\sigma)Q_-^{(\alpha)}(\sigma,T,\rho^{(0)};\mathcal{X})\right]. \tag{65}$$

Solution of the set of Eqs. (58)–(65) for a given temperature T, density of the parent phase $\rho^{(0)}$, and parent distribution function $F_{\pm}^{(0)}(\sigma)$ gives the coexisting densities $\rho^{(\alpha)}$ of the two daughter phases and corresponding distribution functions $F_{\pm}^{(\alpha)}(\sigma)$, $\alpha=1$, 2. The coexistence densities for different temperatures fix binodals, which are terminated at a temperature for which the density of one of the phases is equal to the density $\rho^{(0)}$ of the parent phase; these termination points form the so-called cloud and shadow curves which thus represent an envelope for the binodals. Cloud and shadow curves intersect at the critical point, which is characterized by the critical temperature T_{cr} and critical density $\rho_{cr}=\rho^{(1)}=\rho^{(2)}=\rho^{(0)}$. Thus only for $\rho^{(0)}=\rho_{cr}$ the two branches of the binodal meet at the critical point.

By definition, states located on the cloud curve are characterized that they coexist with a state (localized on the shadow curve) where an infinitely small amount of the other phase emerges. Thus the cloud and shadow curves can be obtained as special solutions of the general phase coexistence problem, when the properties of one phase are equal to the properties of the parent phase: assuming, e.g., the second phase to be the cloud phase, i.e., $\rho^{(2)}=\rho^{(0)}$, and following the scheme presented above we will end up with the same set of equations, (58)–(65), but with $\rho^{(2)}$ and $F_{\pm}^{(2)}(\sigma)$ substituted by $\rho^{(0)}$ and $F_{\pm}^{(0)}(\sigma)$, respectively. Note that $F_{\pm}^{(2)}(\sigma) = F_{\pm}^{(0)}(\sigma)$ is now known, but the remaining properties, i.e., $\rho^{(0)}$, $\Gamma^{(0)}$, and the generalized moments $\{\zeta_n^{(0)}\}$, $\Omega^{(0)}$, and $D^{(0)}$ are unknown; they are obtained from the solution of the appropriately modified set of Eqs. (58)–(65).

Solution of the set of Eqs. (58)–(65) was obtained by using the Newton–Raphson method: we start at a relatively high temperature and a small degree of polydispersity. As the initial input we have used the values of $\Gamma^{(\alpha)}$ and $\rho^{(\alpha)}$, $\alpha=1$,

2, which are obtained from the solution of the phase equilibrium problem for the corresponding monodisperse system; furthermore we assume as starting values for the two daughter distribution functions the parent distribution function, i.e., $F_\pm^{(1)}(\sigma) = F_\pm^{(2)}(\sigma) = F_\pm^{(0)}(\sigma)$. Solution of the set of equations is then obtained by gradually lowering the temperature and increasing the polydispersity.

D. The distributions

So far in our discussion we have not specified the particular functional form of the distribution function of the parent phase. In this study we have chosen beta-distributions for the $f_\pm^{(0)}(\sigma)$, given by

$$f_\pm^{(0)}(\sigma) = B^{-1}(\gamma_\pm, \nu_\pm) \left(\frac{\sigma}{\sigma_\pm^{(\max)}} \right)^{\gamma_\pm - 1}$$
$$\times \left(1 - \frac{\sigma}{\sigma_\pm^{(\max)}} \right)^{\nu_\pm - 1} \Theta(\sigma_\pm^{(\max)} - \sigma)\Theta(\sigma), \quad (66)$$

where

$$\Theta(x) = \begin{cases} 1, & x \geq 0 \\ 0, & x < 0 \end{cases}$$

is the Heaviside step function. The $f_\pm^{(0)}(\sigma)$ are thus different from zero only for $\sigma \in [0, \sigma_\pm^{(\max)}]$. $B(\gamma_\pm, \nu_\pm)$ is the beta-function[43] and the $\gamma_\pm$ and $\nu_\pm$ are related to the first ($\sigma_\pm^{(0)} = \langle\sigma\rangle_\pm^{(0)}$) and second ($\langle\sigma^2\rangle_\pm^{(0)}$) moments—see also Eq. (43)—by

$$\gamma_\pm = \frac{\sigma_\pm^{(\max)} - \sigma_\pm^{(0)}(1 + D_\pm^{(0)})}{\sigma_\pm^{(\max)} D_\pm^{(0)}}, \quad (67)$$

$$\nu_\pm = \left(\frac{\sigma_\pm^{(\max)} - \sigma_\pm^{(0)}}{\sigma_\pm^{(0)}} \right) \gamma_\pm \quad (68)$$

with

$$D_\pm^{(0)} = \langle\sigma^2\rangle_\pm^{(0)}/(\langle\sigma\rangle_\pm^{(0)})^2 - 1; \quad (69)$$

the $D_\pm^{(0)}$ have the same meaning as D_σ in Ref. 44 and correspond to $(1/\alpha)$ in Ref. 39. The choice of a beta-distribution (instead of, for instance, a Schulz-distributions) was motivated and justified in Sec. II C of Ref. 33.

III. RESULTS

A. Numerical procedure and analysis

Solution of the set of Eqs. (49), (52), (53), and (56), along with Eq. (57) leads to the binodal curves and to the distribution functions of the coexisting two daughter phases for the given value of the parent phase density $\rho^{(0)}$ and a given parent distribution function $F^{(0)}(\sigma, z)$. For this solution we have used the same numerical procedure as for the polydisperse HSY system, outlined in Ref. 33. This also holds for the determination of the cloud and the shadow curves and for the critical points. Further we have analyzed the shapes of the daughter distribution functions $f_\pm^{(\alpha)}(\sigma)$ by finding the "closest" beta-distributions $f_\pm^{(\alpha);\text{beta}}(\sigma)$ in the fol-
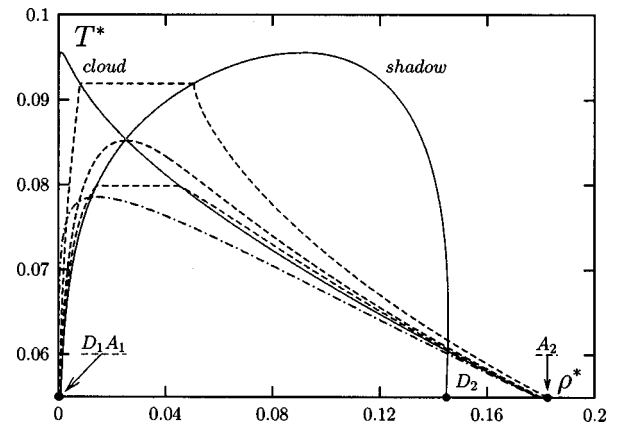

FIG. 1. Phase diagram (T^* vs ρ^*) of the symmetric polydisperse CHS mixture (system I) specified in the text. Cloud and shadow curves are represented by the solid lines (as labeled), binodals by the broken lines: the values of the densities of the respective parent phase, $\rho^{*(0)}$, can be identified from the intersection of the binodal with the cloud curve: $\rho^{*(0)} = 0.008$, 0.045, and 0.0252 (critical binodal). Two pairs of points (A_α and D_α, $\alpha = 1, 2$) are chosen on the $[\rho^{*(0)} = 0.008]$-binodal and on the shadow curve which are specified in Table I. The dashed–dotted line denotes the binodal curve for a RPM [with diameter $\sigma^{(0)}$] treated within the MSA.

lowing way: taking the $f_\pm^{(\alpha)}(\sigma)$ that we obtain from the solution of the above set of equations we calculate directly the first moments, $\langle\sigma\rangle_\pm^{(\alpha)}$, and the $D_\pm^{(\alpha)}$ via Eq. (69); these parameters fix via Eqs. (67) and (68) the parameters of $f_\pm^{(\alpha);\text{beta}}(\sigma)$.

B. The systems

The above formalism has been applied to two polydisperse CHS mixtures. In both models the parent distribution functions $F^{(0)}(\sigma, z) = F^{(0)}(\sigma)$ have the form (42); the partial distribution functions $f_\pm^{(0)}(\sigma)$ are beta-distributions (66). The input parameters for $F^{(0)}(\sigma)$ and for the $f_\pm^{(0)}(\sigma)$ were chosen to be $|z_\pm^{(0)}| = 1$, $\sigma_\pm^{(\max)} = 2\sigma_+^{(0)}$, and $D_\pm^{(0)} = 0.01$:

(i)　The first system (I), is a polydisperse symmetric CHS mixture which can be considered as a generalization of the RPM to the polydisperse case; obviously $\sigma_-^{(0)} = \sigma_+^{(0)}$;

(ii)　The second system (II), is a polydisperse mixture of CHS which is asymmetric in size; it can be considered as a polydisperse extension of the 1:1 electrolyte primitive model with an asymmetry in the size of the HS particles; here we chose $\sigma_-^{(0)} = 1.3\sigma_+^{(0)}$.

In what follows the temperature T and the densities ρ of the system will be represented by the dimensionless quantities $T^* = k_B T \epsilon / e^2$ and $\rho^* = \rho[\sigma_+^{(0)}]^3$, respectively. The indi-

TABLE I. Specification of two selected pairs of points (index 1, low-density gas phase; index 2, high-density fluid phase) chosen in the phase diagram of our symmetric polydisperse CHS mixture (system I) shown in Fig. 1.

Point	Localized on	T^*	$\rho^{*(1)}$	$\rho^{*(2)}$
A_1, A_2	binodal curve [$\rho^{*(0)} = 0.008$]	0.055	$0.512 \cdot 10^{-3}$	0.182
D_1, D_2	cloud and shadow curve	0.055	$0.100 \cdot 10^{-11}$	0.145

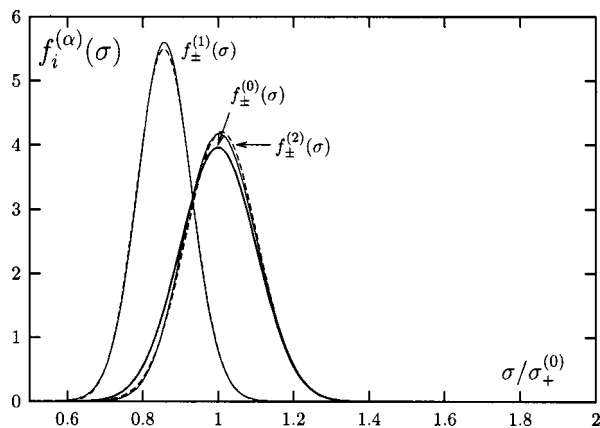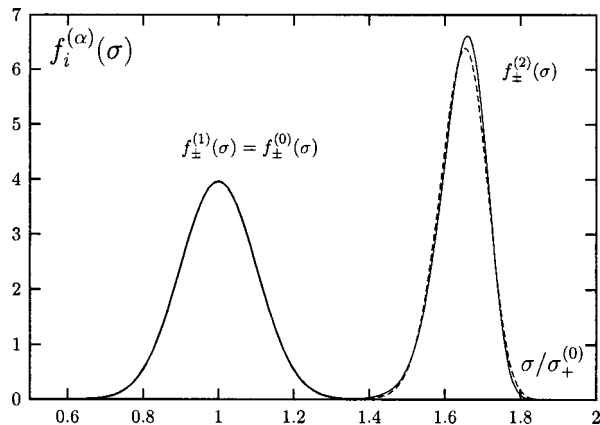FIG. 2. Parent $[f_\pm^{(0)}(\sigma)]$ (thick full line) and daughter $[f_\pm^{(\alpha)}(\sigma), \alpha=1, 2]$ distribution functions (full lines) for the symmetric polydisperse CHS mixture (system I) calculated for points A_1 and A_2, located on the $[\rho^{*(0)}=0.008]$-binodal in the phase diagram (see Table I and Fig. 1). Broken lines: $f_\pm^{(\alpha);\text{beta}}(\sigma)$ as defined in the text. $\alpha=1$, gas phase; $\alpha=2$, fluid phase.

ces $\alpha=1, 2$, specifying the daughter phases, are fixed as follows: index 1 will refer to the low-density (gas) phase, while index 2 will refer to the high-density (fluid) phase.

C. Results for system I

The phase diagram of system I is shown in Fig. 1. We show the cloud and the shadow curves, along with three binodals for three selected densities, one of them being the critical density, $\rho_{cr}^* = 0.0252$. On the shadow curve and the binodal for $\rho^{*(0)}=0.008$ pairs of points have been chosen (labeled by A_α, and D_α, $\alpha=1, 2$) which are specified in Table I; for these pairs of points the daughter distribution functions are displayed in the subsequent Figs. 2 and 3 and are discussed in the text. We also display in the phase diagram the binodal for the RPM calculated in the MSA as a reference curve.

We observe that polydispersity obviously shifts the critical point both to higher densities as well as to higher temperatures: $\rho_{cr}^* = 0.0252$ and $T_{cr}^* = 0.0853$ in the polydisperse
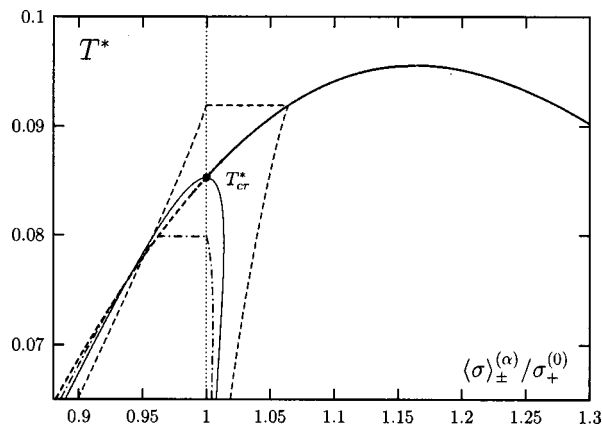

FIG. 4. $\langle\sigma\rangle_\pm^{(\alpha)}$, $\alpha=1, 2$, as defined in Eq. (43) for the symmetric polydisperse CHS mixture (system I) along three binodals for the parent phase densities $\rho^{*(0)}=0.008$ (broken line), $\rho^{*(0)}=\rho_{cr}^*=0.0252$ (full line), $\rho^{*(0)}=0.045$ (dashed–dotted line), and along the shadow curve (thick full and thick broken line). The dotted vertical line through $\langle\sigma\rangle_\pm^{(\alpha)}/\sigma_+^{(0)}=1$ separates the gas (left) from the fluid (right) region. Note that this vertical line represents the $\langle\sigma\rangle_\pm^{(\alpha)}/\sigma_+^{(0)}$-values for states on the cloud curve.

case vs $\rho_{cr;RPM}^* = 0.0144$ and $T_{cr;RPM}^* = 0.0786$ in the case of the RPM. It is also evident that the maximum of the cloud curve is shifted to very small densities: it is located at $\rho^* \sim 0.0011$. The way how the cloud curve varies with the width of the parent distribution function becomes evident, if we bear in mind that the one component system is the limiting case of the polydisperse mixture with an infinitely sharp distribution; thus, broadening the parent distribution function will shift the cloud curve to even smaller densities. The daughter distribution functions of the state points A_α and D_α, $\alpha=1, 2$, are shown in Figs. 2 and 3, which give us a first impression of fractionation effects: as expected, the small particles prefer the gas phase, while the larger particles are predominantly encountered in the fluid phase. We also observe the remarkable fact that both daughter distribution functions $f_\pm^{(\alpha)}(\sigma)$ can be represented reasonably well by

FIG. 3. Parent $[f_\pm^{(0)}(\sigma)]$ (thick full line) and daughter $[f_\pm^{(\alpha)}(\sigma), \alpha=1, 2]$ distribution functions (full lines) for the symmetric polydisperse CHS mixture (system I) calculated for points D_1 and D_2, located on the shadow curve (see Table I and Fig. 1). Broken lines: $f_\pm^{(\alpha);\text{beta}}(\sigma)$ as defined in the text. $\alpha=1$, gas phase; $\alpha=2$, fluid phase.
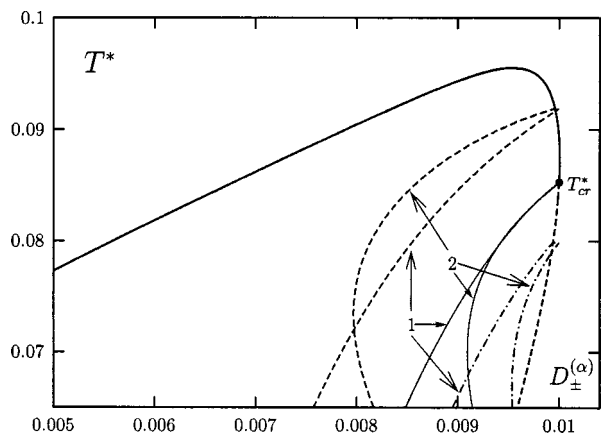

FIG. 5. $D_\pm^{(\alpha)}$, $\alpha=1, 2$, as defined in the text (69) for the symmetric polydisperse CHS mixture (system I) along three binodals for the parent phase densities $\rho^{*(0)}=0.008$ (broken line), $\rho^{*(0)}=\rho_{cr}^*=0.0252$ (full line), and $\rho^{*(0)}=0.045$ (dashed–dotted line) and along the shadow curve (thick full and thick broken line). Binodals: $\alpha=1$, gas phase; $\alpha=2$, fluid phase; shadow curve: broken line, gas phase; full line, fluid phase.
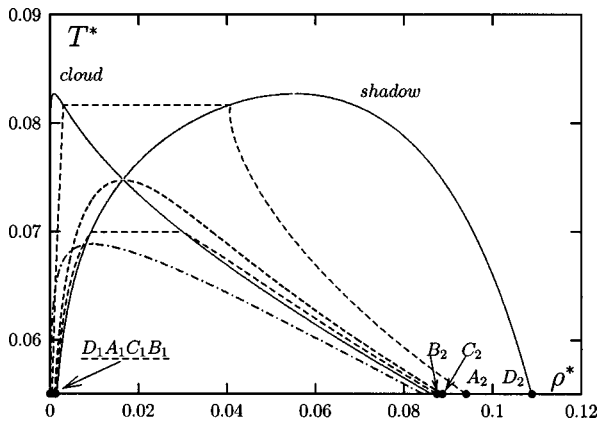
J. Chem. Phys., Vol. 120, No. 21, 1 June 2004

Phase coexistence in a polydisperse fluid   10141

FIG. 6. Phase diagram (T^* vs ρ^*) of the asymmetric polydisperse CHS mixture (system II) specified in the text. Cloud and shadow curves are represented by the solid lines (as labeled), binodals by the broken lines: the values of the densities of the respective parent phase can be identified from the intersection of the binodal with the cloud curve: $\rho^{*(0)} = 0.003, 0.03$, and 0.0165 (critical binodal). Four pairs of points (A_α, B_α, C_α, and D_α, $\alpha = 1$, 2) are chosen on the three different $\rho^{*(0)}$-binodals and on the shadow curve which are specified in Table II. The dashed–dotted line denotes the binodal curve for an asymmetric binary mixture of CHS [with diameters $\sigma_+^{(0)}$ and $\sigma_-^{(0)}$] treated within the MSA.
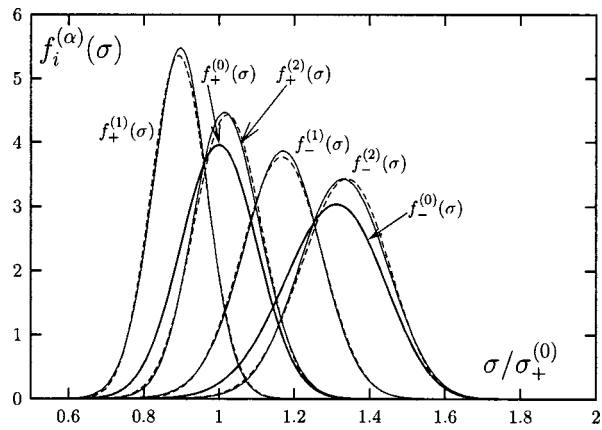

FIG. 7. Parent [$f_i^{(0)}(\sigma), i = +, -$] (thick full lines) and daughter [$f_i^{(\alpha)}(\sigma)$, $i = +, -$ and $\alpha = 1, 2$] distribution functions (full lines) for the asymmetric polydisperse CHS mixture (system II) calculated for points A_1 and A_2, located on the [$\rho^{*(0)} = 0.003$]-binodal in the phase diagram (see Table II and Fig. 6). Broken lines: $f_\pm^{(\alpha);\text{beta}}(\sigma)$ as defined in the text. $\alpha = 1$, gas phase; $\alpha = 2$, fluid phase.

beta-distributions $f_\pm^{(\alpha);\text{beta}}(\sigma)$, $\alpha = 1$, 2; this holds not only for the examples shown here but also for further state points not displayed here.

A more quantitative and systematic analysis of the daughter distribution functions is possible in terms of $\langle\sigma\rangle_\pm^{(\alpha)}$ and $D_\pm^{(\alpha)}$, as defined in Eqs. (43) and (69), i.e., the parameters that characterize the position of the maximum and the width of the $f_\pm^{(\alpha)}(\sigma)$; they are displayed in Figs. 4 and 5 for three chosen densities of the parent phase [i.e., $\rho^{*(0)} = 0.008$, $\rho^{*(0)} = 0.045$, and the critical density, $\rho_{\text{cr}}^{*(0)} = 0.0252$] and along the shadow curve. Along the shadow curve, fractionation has its strongest effects: the smaller particles are preferentially in the gas phase while the larger ones are predominantly encountered in the fluid phase; the width of the daughter distributions in the fluid phase, $D_\pm^{(2)}$, is considerably smaller than the width of the parent distribution, while in the gas phase $D_\pm^{(1)}$ is only slightly smaller than $D_\pm^{(0)}$. Looking on the temperature dependence of the mean-size of the particles in the daughter phases along the three binodals we observe the following: in the gas phase we remark a strong decrease of the mean particle size, $\langle\sigma\rangle_\pm^{(1)}$, with temperature (where this effect is smaller for smaller densities); in the fluid phase, we observe different temperature dependencies of $\langle\sigma\rangle_\pm^{(2)}$: for densities larger than the

critical density the mean size is monotonically increasing as the temperature decreases, while we find the opposite tendency for $\rho < \rho_{\text{cr}}^*$. As we further decrease the temperature, the liquid branches of these curves become nearly vertical, which means that for lower temperatures the mean particle size in the fluid daughter phase does not change anymore. The $D_\pm^{(\alpha)}$-curves along the three binodals as functions of the temperature indicate a strong influence both of density and temperature on the width of the daughter distributions: while for densities above ρ_{cr}^* the width of the distribution function of the gas phase is always smaller than the one of the fluid phase, this is not the case for densities below the critical density: here $D_\pm^{(2)}$ (fluid phase) may even be smaller than $D_\pm^{(1)}$ (gas phase), leading to a looplike shape of the $D_\pm^{(\alpha)}$-curves. For all binodals investigated, $D_\pm^{(\alpha)}$, $\alpha = 1$, 2, is smaller than the corresponding value of the parent phase, $D_\pm^{(0)} = 0.01$. Finally, we have analyzed the average (positive or negative) charge of the daughter phases as functions of the temperature. They show a similar behavior as the $\langle\sigma\rangle_\pm^{(\alpha)}$ and are therefore not displayed here; this fact is undoubtedly re-
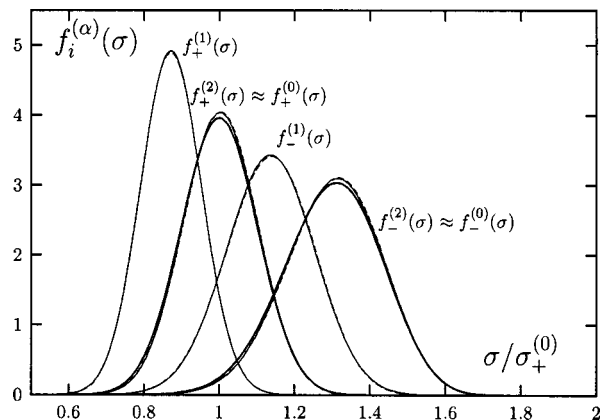
TABLE II. Specification of four selected pairs of points (index 1, low-density gas phase; index 2, high-density fluid phase) chosen in the phase diagram of our asymmetric polydisperse CHS mixture (system II) shown in Fig. 6.

Point	Localized on	T^*	$\rho^{*(1)}$	$\rho^{*(2)}$
A_1, A_2	binodal curve [$\rho^{*(0)} = 0.003$]	0.055	$0.552 \cdot 10^{-3}$	0.094
B_1, B_2	binodal curve [$\rho^{*(0)} = 0.03$]	0.055	$0.132 \cdot 10^{-2}$	0.087
C_1, C_2	critical binodal ($\rho_{\text{cr}}^* = 0.0165$)	0.055	$0.113 \cdot 10^{-2}$	0.089
D_1, D_2	cloud and shadow curve	0.055	$0.300 \cdot 10^{-8}$	0.109

FIG. 8. As Fig. 7 for points B_1 and B_2 located on the [$\rho^{*(0)} = 0.03$]-binodal in the phase diagram of system II (see Table II and Fig. 6).
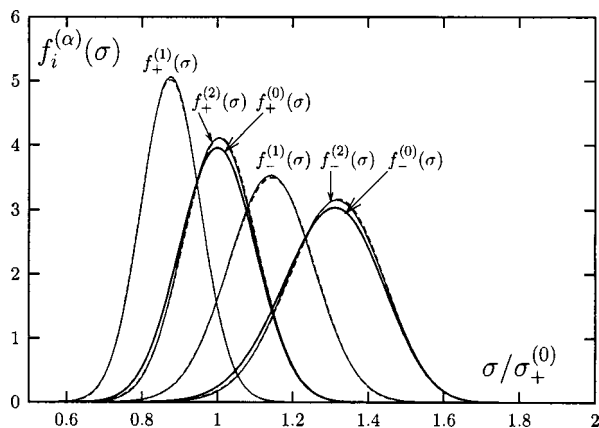
FIG. 9. As Fig. 7 for points C_1 and C_2 located on the critical binodal (ρ^*_{cr} =0.0165) in the phase diagram of system II (see Table II and Fig. 6).

FIG. 11. $\langle\sigma\rangle_i^{(\alpha)}$, $i=+,-$ (as labeled) and $\alpha=1, 2$, as defined in Eq. (43) for the asymmetric polydisperse CHS mixture (system II) along the shadow curve. Broken line ($\alpha=1$), gas phase; full line ($\alpha=2$), fluid phase.

lated to the size-charge dependence assumed in our model (42).

D. Results for system II

In system II the situation is of course—as a consequence of the asymmetry—more complex. Again, we start with the phase diagram which is depicted in Fig. 6: we show the cloud and shadow curves, the critical binodal (ρ^*_{cr} =0.0165), and two further binodals with their respective densities of the parent phase below and above ρ^*_{cr} [i.e., $\rho^{*(0)}$=0.003, $\rho^{*(0)}$=0.03]. Four pairs of points (A_α, B_α, C_α, and D_α, $\alpha=1, 2$) have now been chosen on these curves; they are indicated in Fig. 6 and are characterized in Table II.

Similar as in the symmetric case, the cloud curve has a maximum for a very small ρ^*-value; again, we have complemented the results by the binodal of an asymmetric 1:1 primitive model [with diameters $\sigma_+^{(0)}$ and $\sigma_-^{(0)}$] treated within the MSA and we observe that the critical point of the polydisperse mixture is shifted to higher densities and temperatures: ρ^*_{cr}=0.0165 and T^*_{cr}=0.0075 in the polydisperse case vs $\rho^*_{cr;bin}$=0.0096 and $T^*_{cr;bin}$=0.069.

The analysis of the daughter distribution functions $f_\pm^{(\alpha)}(\sigma)$ displayed in Figs. 7–10 is of course now more di-
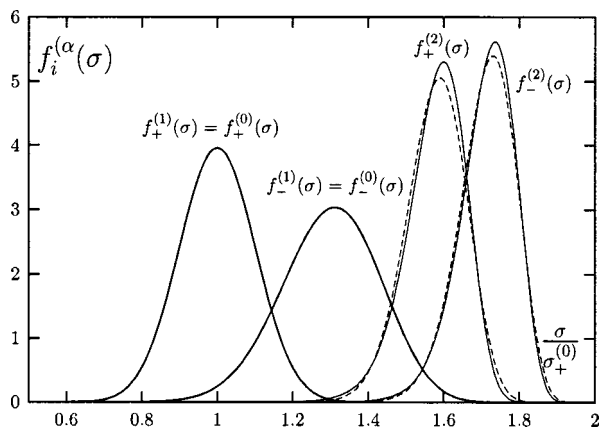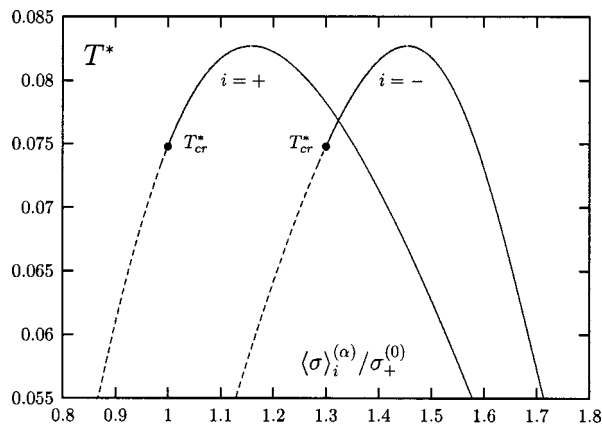
versified since due to the asymmetry of the model $f_+^{(\alpha)}(\sigma)$ $\neq f_-^{(\alpha)}(\sigma)$. Similar to the symmetric case and to the study on the polydisperse HSY mixture[33] we observe that *all four* daughter distribution functions can be represented reasonably well by beta-distributions with suitably chosen parameters $\langle\sigma\rangle_\pm^{(\alpha)}$ and $D_\pm^{(\alpha)}$; again this has been investigated and substantiated for more state points than presented here.

We continue with a more quantitative and a more detailed analysis of the distribution functions of the daughter phases in terms of the $\langle\sigma\rangle_\pm^{(\alpha)}$ and $D_\pm^{(\alpha)}$. For the $\langle\sigma\rangle_\pm^{(\alpha)}$-curves in the daughter phases (Figs. 11 and 12) we find similar shapes as in the symmetric case, the + and − curves being now located "around" their respective values of the parent phases $\sigma_+^{(0)}$=1.0 and $\sigma_-^{(0)}$=1.3. The situation is different for the width of the distributions, $D_+^{(\alpha)}$ and $D_-^{(\alpha)}$ (Figs. 13 and 14): along the shadow curve, $D_+^{(\alpha)}$ remains— except for $\rho^{*(0)}$-values close to the critical densities— smaller than 0.01, i.e., the $D_\pm^{(0)}$-value of the parent phase. For the negative particles, the width of the daughter distribu-
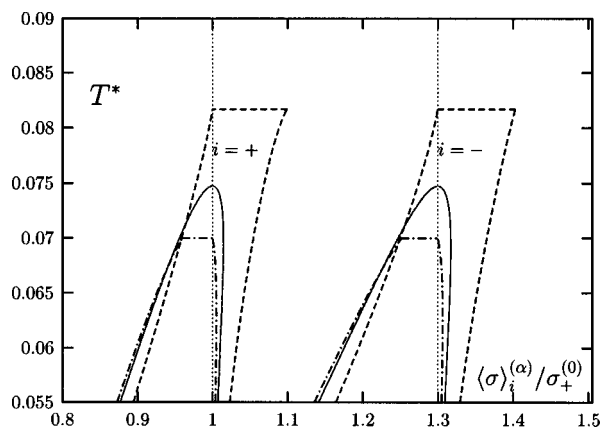

FIG. 12. $\langle\sigma\rangle_i^{(\alpha)}$, $i=+,-$ (as labeled) and $\alpha=1, 2$, as defined in Eq. (43) for the asymmetric polydisperse CHS mixture (system II) along three binodals for the parent phase densities $\rho^{*(0)}$=0.003 (broken line), $\rho^{*(0)}$=ρ^*_{cr} =0.0165 (full line), and $\rho^{*(0)}$=0.03 (dashed–dotted line). The two dotted vertical lines through $\langle\sigma\rangle_+^{(\alpha)}/\sigma_+^{(0)}$=1 and $\langle\sigma\rangle_-^{(\alpha)}/\sigma_+^{(0)}$=1.3 separate the respective gas (left) from the fluid (right) regions. Note that these vertical lines represent the $\langle\sigma\rangle_i^{(\alpha)}$-values, $i=+,-$, for states on the cloud curve.

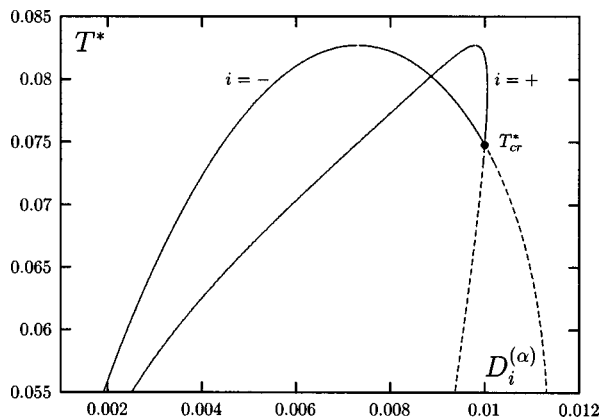FIG. 10. As Fig. 7 for points D_1 and D_2 located on the shadow curve of system II (see Table II and Fig. 6).

FIG. 13. $D_i^{(\alpha)}$, $i=+,-$ (as labeled) and $\alpha=1, 2$, as defined in Eq. (69) for the asymmetric polydisperse CHS mixture (system II) along the shadow curve. Broken line ($\alpha=1$), gas phase; full line ($\alpha=2$), fluid phase.
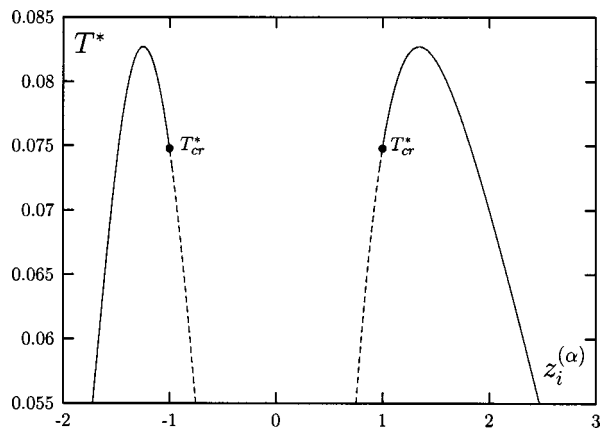

FIG. 15. Average positive $z_+^{(\alpha)}$ and negative $z_-^{(\alpha)}$ charges, $\alpha=1, 2$, for the asymmetric polydisperse CHS mixture (system II) along the shadow curve. Broken line ($\alpha=1$), gas phase; full line ($\alpha=2$), fluid phase.

tion function in the gas phase is larger than 0.01, while in the liquid phase $D_-^{(2)}$ is always smaller than $D_\pm^{(0)}=0.01$. Along the three binodals the situation is also more complex than in the symmetric case: the $D_+^{(\alpha)}$-curves show a similar behavior as observed in the symmetric case, i.e., $D_+^{(\alpha)}$ is always smaller than $D_\pm^{(0)}$ and for densities smaller than ρ_{cr}^* a loop-like shape may occur. This also holds for $\rho<\rho_{cr}^*$ for the $D_-^{(\alpha)}$-curves. However, for $\rho\geqslant\rho_{cr}^*$, $D_-^{(1)}$ (gas phase branch) may become larger than the width of the parent distribution function, $D_\pm^{(0)}=0.01$.

We finally turn towards the influence of the phase separation process on the average charges and on the fraction of the positive and negative charges of the coexisting phases: in Figs. 15 and 16 we show the average positive and negative charges, $z_\pm^{(\alpha)}$, $\alpha=1, 2$, for state points on the shadow curve and on the three binodals considered in this study. The curves are rather narrow and are centered around the $z_\pm^{(0)}$-values of ±1; this means that the charges do not vary too much as we change the temperature and the density of the parent phase. The respective $z_+^{(\alpha)}$- and $z_-^{(\alpha)}$-curves seem rather "symmetric" with respect to 0; thus we can conclude

that the size difference affects the charge distribution only marginally. As we lower the temperature, the charges of the fluid phase tend towards ±1. Along the shadow curves the average charges very somewhat stronger than along the binodals. Finally, in Figs. 17 and 18 we display the fraction of positive particles in the two phases, expressed by $\alpha_+^{(\alpha)}$: from the results along the shadow curve (Fig. 17) we observe that in the gas daughter phase a slight majority of positive particles can be observed while in the fluid phase, $\alpha_+^{(2)}$ is less than 0.5. This effect is more pronounced and diversified for the three binodals for the three different densities considered (Fig. 18): in the fluid phase (where the larger particles are predominantly encountered) the fraction of positive particles is always smaller than 0.5 (although the maximum deviation from this value for the systems investigated here is only 0.01). On the other hand, in the gas phase the positive particles have a slight majority (up to ~0.0502). As we decrease the temperature, the density dependence of the $\alpha_+^{(\alpha)}$-curves vanishes and the curves tend towards 0.5. Note that the curves of Figs. 16 and 18 reflect—along with $\alpha_+^{(\alpha)}+\alpha_-^{(\alpha)}=1$, $\alpha=1, 2$—the charge neutrality condition (48).
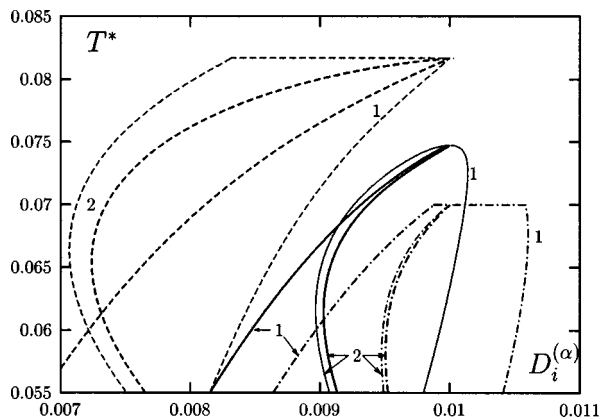

FIG. 14. $D_i^{(\alpha)}$, $i=+,-$ and $\alpha=1, 2$, as defined in Eq. (69) for the asymmetric polydisperse CHS mixture (system II) along three binodals for the parent phase densities $\rho^{*(0)}=0.003$ (broken lines), $\rho^{*(0)}=\rho_{cr}^*=0.0165$ (full lines), and $\rho^{*(0)}=0.03$ (dashed–dotted lines). Thick lines, $D_+^{(\alpha)}$; thin lines, $D_-^{(\alpha)}$; $\alpha=1$ gas phase; $\alpha=2$, fluid phase.
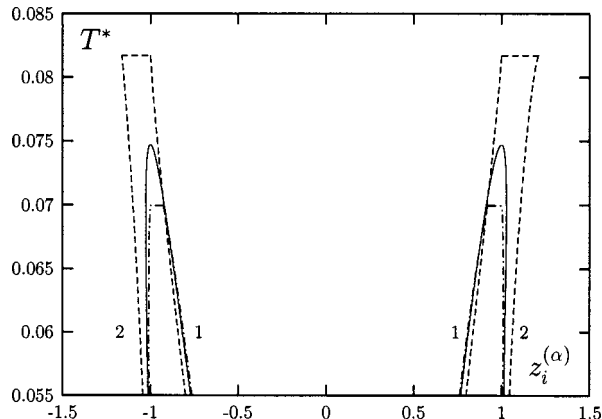

FIG. 16. Average positive $z_+^{(\alpha)}$ and negative $z_-^{(\alpha)}$ charges, $\alpha=1, 2$, for the asymmetric polydisperse CHS mixture (system II) along three binodals with the parent phase densities $\rho^{*(0)}=0.003$ (broken line), $\rho^{*(0)}=\rho_{cr}^*=0.0165$ (full line), and $\rho^{*(0)}=0.03$ (dashed–dotted line). $\alpha=1$, gas phase; $\alpha=2$, fluid phase.
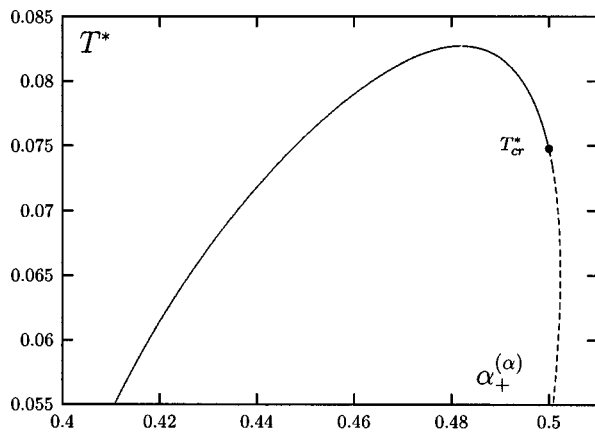
FIG. 17. Fraction of positive charges, $\alpha_+^{(\alpha)}$, $\alpha=1$, 2, for the asymmetric polydisperse CHS mixture (system II) along the shadow curve. Broken line ($\alpha=1$), gas phase, full line ($\alpha=2$), fluid phase.

IV. CONCLUSIONS

In this contribution we have shown that a polydisperse mixture of CHS treated within the MSA also belongs to the class of truncatable free energy models, i.e., to those systems where the thermodynamic properties can be expressed with a finite set of generalized moments of the distribution function characterizing the system. We have presented explicit expressions for the thermodynamic properties in terms of these moments, taking into account the constraints of charge neutrality, total volume conservation, and conservation of the total number of particles of each species. Restricting ourselves to two-phase coexistence, the equations that determine the parameters of the two coexisting phases were derived which turn out to be a set of fifteen coupled, nonlinear equations in the unknown moments of the daughter phases. At its present level, the formalism is still simplified in the sense that we assume a simple relation between the two independent variables that characterize the system, i.e., size and charge, via a physically sound choice: for each particle the charge is proportional to its surface.

Via this route, the problem of calculating the phase diagram of a polydisperse mixture of CHS has become trac-

table. Having implemented this formalism we were able to solve the coexistence equations by means of an efficient and reliable numerical algorithm, based on a Newton–Raphson method. We demonstrate the power of this approach by considering two polydisperse mixtures of CHS, one being symmetric (being thus a polydisperse generalization of the RPM), the other being asymmetric in size. The size of the particles of the parent phases is assumed to be distributed according to beta-distributions. We are able to calculate the full phase diagram in terms of cloud and shadow curves as well as binodals, each of these being characterized by density values of the parent phase. We observe that with respect to the corresponding one- or two-component system, the critical point is shifted towards higher temperatures and higher densities. A closer analysis of the daughter distribution functions in terms of their width and the mean size of the particles in each phase gives a quantitative insight into fractionation effects. The formalism allows furthermore to determine the average charge and the fraction of positive and negative particles in each of the coexisting phases (charge fractionation). From these analyses we observe—despite the simple parent distribution function used and the simple relation between size and charge of the particles—a rather rich variety of phenomena.
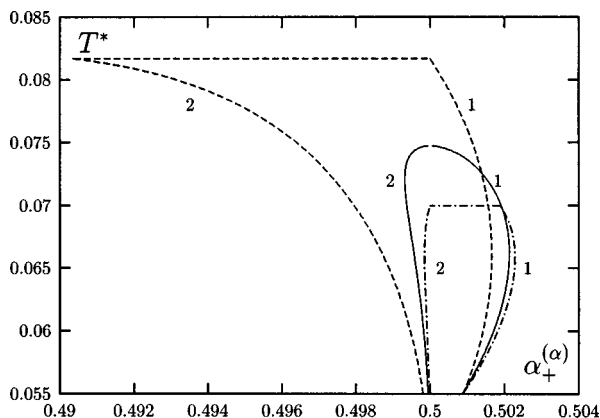
ACKNOWLEDGMENTS

FIG. 18. Fraction of positive charges, $\alpha_+^{(\alpha)}$, $\alpha=1$, 2, for the asymmetric polydisperse CHS mixture (system II) along three binodals with the parent phase densities $\rho^{*(0)}=0.003$ (broken line), $\rho^{*(0)}=\rho_{cr}^*=0.0165$ (full line), and $\rho^{*(0)}=0.03$ (dashed–dotted line). $\alpha=1$, gas phase; $\alpha=2$, fluid phase.

[1] F. Stillinger and R. Lovett, J. Chem. Phys. **48**, 3858 (1968).
[2] W. Ebeling, Z. Phys. Chem. (Leipzig) **247**, 340 (1971).
[3] G. Stell, K. C. Wu, and B. Larsen, Phys. Rev. Lett. **37**, 1369 (1976).
[4] N. P. Vorontsov-Veliaminov, A. M. El'yashevich, L. A. Morgenshtern, and V. P. Chasovskikh, Teplofiz. Vys. Temp. **8**, 277 (1970).
[5] A. Z. Panagiotopoulos, Fluid Phase Equilib. **76**, 97 (1992).
[6] J.-M. Caillol, J. Chem. Phys. **100**, 2161 (1994).
[7] G. Orkoulas and A. Z. Panagiotopoulos, J. Chem. Phys. **101**, 1452 (1994).
[8] J.-M. Caillol and J.-J. Weis, J. Chem. Phys. **102**, 7610 (1995).
[9] J.-M. Caillol, D. Levesque, and J.-J. Weis, J. Chem. Phys. **107**, 1565 (1997).
[10] G. Orkoulas and A. Z. Panagiotopoulos, J. Chem. Phys. **110**, 1581 (1999).
[11] J. M. Romero-Enrique, G. Orkoulas, A. Z. Panagiotopoulos, and M. E. Fisher, Phys. Rev. Lett. **85**, 4558 (2000).
[12] A. Z. Panagiotopoulos, J. Chem. Phys. **116**, 3007 (2002).
[13] M. E. Fisher and Y. Levin, Phys. Rev. Lett. **71**, 3826 (1993).
[14] Y. Levin and M. E. Fisher, Physica A **225**, 164 (1996).
[15] Y. Q. Zhou, S. Yeh, and G. Stell, J. Chem. Phys. **102**, 5785 (1995).
[16] S. Yeh, Y. O. Zhou, and G. Stell, J. Phys. Chem. **100**, 1415 (1996).
[17] Yu. V. Kalyuzhnyi, Mol. Phys. **94**, 735 (1998).
[18] J. W. Jiang, L. Blum, and O. Bernard, Mol. Phys. **99**, 1765 (2001).
[19] J. W. Jiang, L. Blum, O. Bernard, J. M. Prausnitz, and S. I. Sandler, J. Chem. Phys. **116**, 7977 (2002).
[20] M. F. Holovko and Yu. V. Kalyuzhnyi, Mol. Phys. **73**, 1145 (1991).
[21] Yu. V. Kalyuzhnyi and M. F. Holovko, Mol. Phys. **80**, 1165 (1993).
[22] G. Stell and Y. Q. Zhou, J. Chem. Phys. **91**, 3618 (1989).
[23] Yu. V. Kalyuzhnyi, M. F. Holovko, and V. Vlachy, J. Stat. Phys. **100**, 243 (2000).
[24] O. Yan and J. J. de Pablo, Phys. Rev. Lett. **86**, 2054 (2001).

J. Chem. Phys., Vol. 120, No. 21, 1 June 2004

Phase coexistence in a polydisperse fluid   10145

[25] D. M. Zukerman, M. E. Fisher, and S. Bekiranov, Phys. Rev. E **64**, 011206 (2001).

[26] J. Reščič and P. Linze, J. Chem. Phys. **114**, 10131 (2001).

[27] Yu. V. Kalyuzhnyi and P. T. Cummings, J. Chem. Phys. **115**, 540 (2001); **116**, 8637(E) (2002).

[28] A. Z. Panagiotopoulos and M. E. Fisher, Phys. Rev. Lett. **88**, 045701 (2002).

[29] O. Yan and J. J. de Pablo, Phys. Rev. Lett. **88**, 095504 (2002).

[30] M. N. Artyomov, V. Kobelev, and A. B. Kolomeisky, J. Chem. Phys. **118**, 6394 (2003).

[31] D. W. Cheong and A. Z. Panagiotopoulos, J. Chem. Phys. **119**, 8526 (2003).

[32] C. Caccamo, Phys. Rep. **274**, 1 (1996).

[33] Yu. V. Kalyuzhnyi and G. Kahl, J. Chem. Phys. **119**, 7335 (2003).

[34] L. Blum, Mol. Phys. **30**, 1529 (1975).

[35] L. Blum and J. S. Høye, J. Phys. Chem. **81**, 1311 (1977).

[36] S. Leroch, Ph.D. thesis, Technische Universität Wien, 2002.

[37] P. Sollich, J. Phys.: Condens. Matter **14**, R79 (2002).

[38] J. A. Gualtieri, J. M. Kincaid, and G. Morrison, J. Chem. Phys. **77**, 521 (1982).

[39] L. Bellier-Castella, H. Xu, and M. Baus, J. Chem. Phys. **113**, 8337 (2000).

[40] L. Bellier-Castella, M. Baus, and H. Xu, J. Chem. Phys. **115**, 3381 (2001).

[41] G. A. Mansoori, N. F. Carnahan, K. E. Starling, and T. W. Leland, J. Chem. Phys. **54**, 1523 (1971).

[42] J. J. Salacuse and G. Stell, J. Chem. Phys. **77**, 3714 (1982).

[43] M. Abramowitz and I. A. Stegun, *Handbook of Mathematical Functions*, Applied Mathematical Series (National Bureau of Standards, Washington, D.C., 1964), Vol. 55.

[44] M. Ginoza and M. Yasutomi, Mol. Phys. **95**, 163 (1998).